*33rd EPS Conference on Plasma Phys. Rome, 19 - 23 June 2006 ECA Vol.**30I**, P-1.044 (2006)*

Real-space statistical characterization of turbulence and transport in the TORPEX experiment

S. H. Müller, A. Diallo, A. Fasoli, I. Furno, B. Labit, G. Plyushchev, M. Podestà, F. M. Poli

Centre de Recherches en Physique des Plasmas, Association EURATOM – Confédération Suisse, CRPP EPFL, Lausanne, Switzerland

Fluctuating structures of plasma density or potential can be identified as objects in real space, whose properties can be measured, and whose dynamics can be followed. The statistical distributions of the related observables provide a robust framework in which the nature of the fluctuations, the turbulence and the related transport can be characterized. A Langmuir probe array for such real-space measurements of fluctuating structures has been installed in the TORPEX toroidal device ($R = 1\,\mathrm{m}$, $a = 0.2\,\mathrm{m}$) [1], in which plasmas are produced using RF waves in the electron cyclotron frequency range in a primarily toroidal magnetic field of $\sim 0.1\,\mathrm{T}$. The array covers the whole poloidal section with 86 tips arranged in a hexagonal grid, providing a spatial resolution of $3.5\,\mathrm{cm}$ [2].

A threshold-segmentation approach [3] is adopted to identify structures as regions exceeding a threshold value, taken symmetrically with respect to the time-average profile. The standard deviation of the concatenated signals of all probes provides a good working value. For each structure, the bounding polygon is found and structure observables, like occupied area, mass, center of mass, orientation and extension are calculated using integral geometrical moments [3]. By virtue of the integrations, finite-resolution effects can be reduced significantly. Trajectories

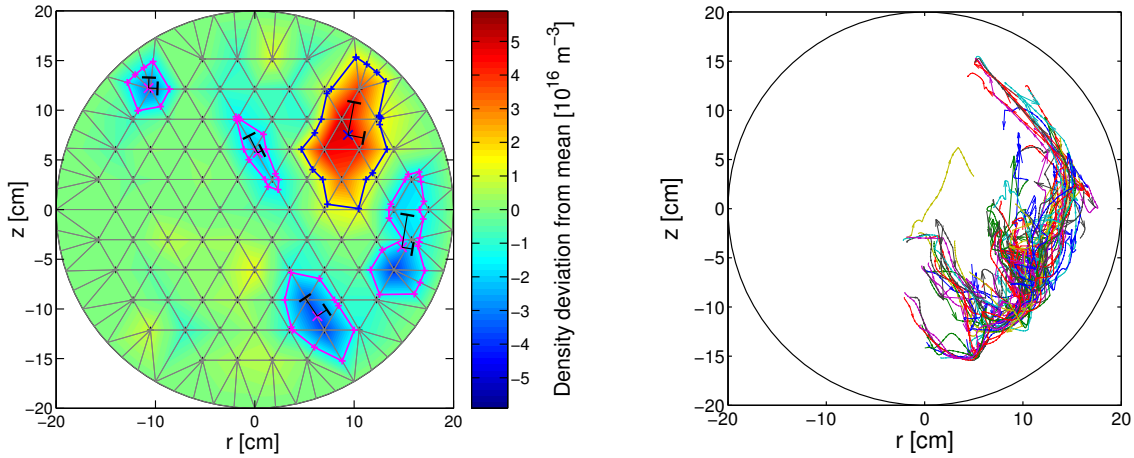

Figure 1: (Left) Snapshot showing non-trivial structure patterns. The bounding polygon, and the extracted structure observables center of mass, orientation and extension are indicated. (Right) Fifty examples of extracted trajectories.

are found by following the identified structures in time using a continuation criterion, and the structure velocities are evaluated by finite differencing along the trajectories. For a discharge of 0.6 s length, corresponding to 150000 time frames sampled at 250 kHz, a database of about 70000 trajectories of positive and negative structures is typically extracted, which is then analyzed statistically. In the following we introduce briefly some statistical questions of interest and the relevant representations of the results.

Trajectory histogram. The poloidal cross section is divided into a grid of 60×60 bins, and the number of trajectories touching each bin is recorded (shown color coded). The ensemble-averaged velocity field $\langle \mathbf{v} \rangle$, where $\langle \cdot \rangle$ denotes an ensemble average obtained by first averaging the quantity for each trajectory in each bin and then averaging over the trajectory realizations, is also shown (blue arrows). Three silver contour lines are drawn at 25%, 50% and 75% of the maximum value of the time-average density profile.

Pilot chart. This analysis technique deals with the statistical properties of structure motion. The domain is divided into a grid of 5×5 quadratical regions. Inside each region, the velocity directions are binned into octants, and the average speed is evaluated for each octant. The result is represented by a blue *rose* in the center of each region. The lengths of the eight arrow shafts, not including the feathers, are proportional to the probability that the velocity direction falls into the corresponding octant. The number of feathers, each standing for 250 m/s, indicates the average speed for each direction. The area of the circle in the center of each rose is proportional to the number of realizations in the region. Light blue L's coding the average structure orientations and extensions are superimposed (compare Fig. 1). The rms fluctuation profile is shown color coded, along with the three isocontours of the average density profile.

Transport chart. To study the structure-induced transport, a grid of macroscopic radial and poloidal surfaces is introduced and transport events are analyzed, characterized by the time when a structure center of mass crosses a surface and by the mass transported through it. The average transport is deduced for each surface and shown color coded (positive: radially outward or poloidally counter-clockwise). The ensemble-averaged flux-density field $\langle \bar{\Gamma} \rangle \equiv \langle \bar{n}\mathbf{v} \rangle$ is superimposed, where $\bar{n}$ is the signed structure-averaged excess density (shown as blue arrows). Three silver contour lines of the time-series skewness profile are also shown.

Overall speed-area joint probability distribution. A histogram estimate of the overall speed-area joint probability distribution is obtained by binning all observed occupied areas and speeds (logarithmically), regardless where they occurred (shown as color coded surface).

Having introduced the necessary framework we discuss the results for a helium and an argon discharge (Fig. 2), with identical external discharge parameters (toroidal magnetic field on axis

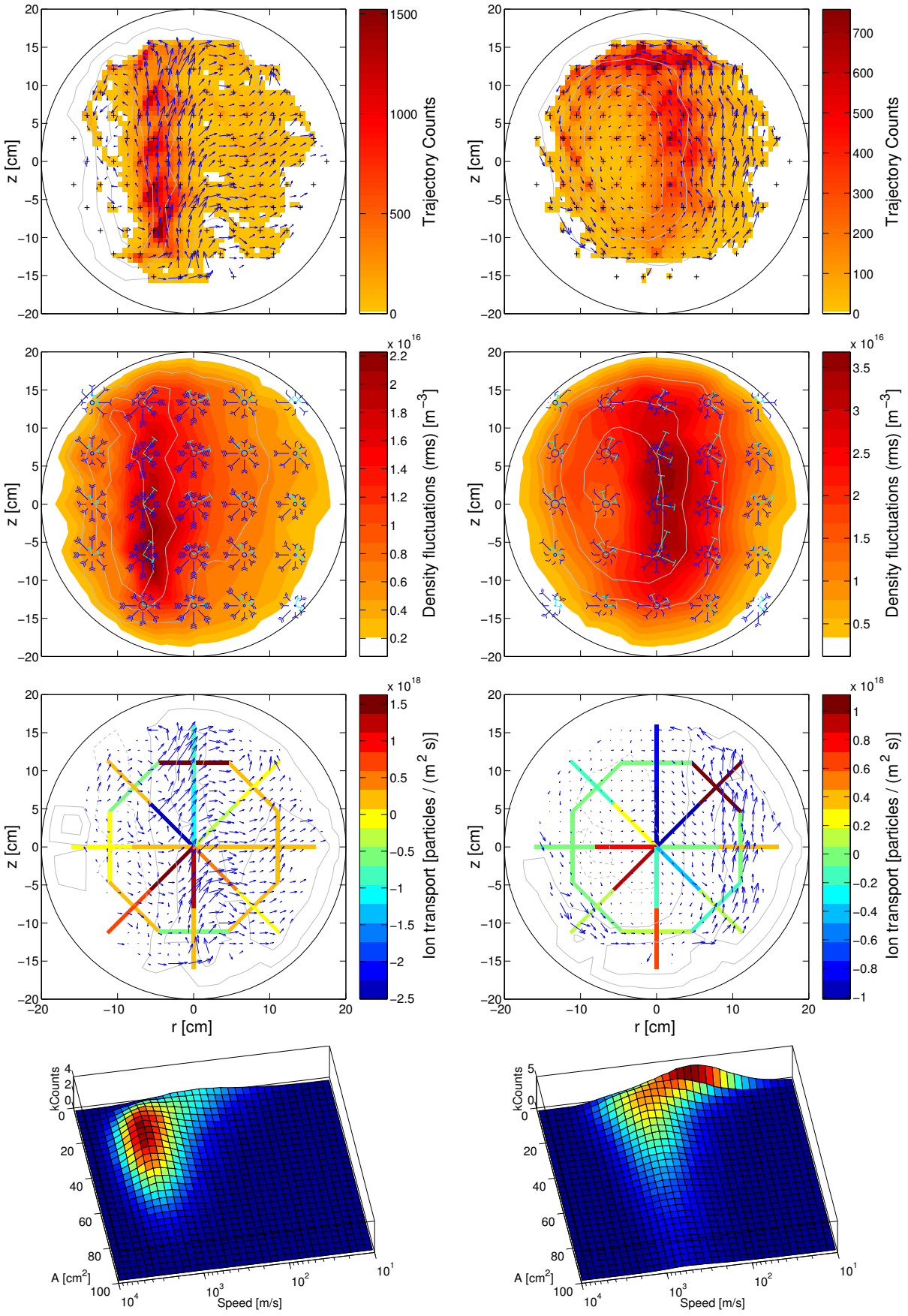

Figure 2: Results for helium (left) and argon (right). From top to bottom: trajectory histogram, pilot chart, transport chart and overall speed-area joint probability distribution.

$\sim 76\,\mathrm{mT}$, vertical magnetic field $1.8\,\mathrm{mT}$, RF power $\sim 300\,\mathrm{W}$, neutral gas pressure $\sim 2.5 \times 10^{-5}\,\mathrm{mbar}$). The maximum densities are $6 \times 10^{16}\,\mathrm{m}^{-3}$ and $11 \times 10^{16}\,\mathrm{m}^{-3}$, respectively. Due to the high vertical magnetic field, about twice the optimal value for particle confinement [4], vertically elongated density profiles form, more pronounced for the helium case than for the argon one. The spectral power of the fluctuations is typically concentrated below 10–20 kHz, where it shows both broadband and narrowband features. The maximum relative rms fluctuation levels lie at approximately 50% for both gases, occurring on the outboard slope of the profile on the bad-curvature side, indicating an interchange-type instability. At this location, structures move vertically up in both cases. However, for helium, a part of the structures move radially outward, while for argon some structures appear to propagate around the profile ridge and go downward on the inboard side. From the analysis of the trajectories it is evident that most of the structures do not travel long distances (i.e. comparable to a), and that the dynamics is best described by a continuous generation, short-distance propagation and disappearance of structures. One remarkable difference between the two gases is given by the speed distributions. While for argon the average speeds lie in the range of 500–1000 m/s, for helium they are about 2–3 times higher. This observation is confirmed also for other helium discharges, but not for hydrogen, in which speeds comparable to the argon case are observed.

The net transport resulting from an imbalance between positive and negative structures, in abundance, size or speeds, reflects the general picture of the trajectory histogram. For helium, a net positive radial transport is evident. However, it must be noted that by measuring the structure masses relative to the time-average profile, the transport evaluated in this way, by definition, cannot account for the macroscopic losses determining the time-average profile itself. Instead, it must be interpreted as the transport that happens on top of a time-average profile, assumed to be static and always there. However, in cases with high fluctuation levels, the time-average loses its significance as a reference point to distinguish the moving part of the profile from the static part, which is assumed not to participate in the structure motion. In such cases it may be more natural to evaluate the transport relative to the vacuum level.

This work is partly supported by the Fonds National Suisse pour la Recherche Scientifique.

References

[1] A. Fasoli, B. Labit, M. McGrath, et al. *Phys. Plasmas*, 13:055902, 2006.

[2] S. H. Müller, A. Fasoli, B. Labit, et al. *Phys. Plasmas*, 12(9):090906, 2005.

[3] M. Sonka, V. Hlavac, and R. Boyle. *Image Processing, Analysis, and Machine Vision*. Brooks/Cole, Pacific Grove, CA 93950, USA, second edition, 1999.

[4] S. H. Müller, A. Fasoli, B. Labit, et al. *Phys. Rev. Lett.*, 93:165003, 2004.